PAPER

Structural and relative stabilities, electronic properties and possible reactive routing of osmium and ruthenium borides from first-principles calculations†

Yachun Wang,[a] Tiankai Yao,[a] Li-Min Wang,[a] Jinlei Yao,[b,c] Hui Li,[a] Jingwu Zhang*[a] and Huiyang Gou*[a,d,e]

First-principles calculations are employed to provide a fundamental understanding of the structural features and relative stability, mechanical and electronic properties and possible reactive route for osmium and ruthenium borides. The structural searches and calculations of the formation enthalpy identify a low-energy monoclinic phase for OsB_3 with $P2_1/m$ symmetry, an orthorhombic phase for OsB_4 with $Pmmn$ symmetry, an orthorhombic phase for RuB_3 with $Pnma$ symmetry and a hexagonal phase for RuB_4 with $P6_3/mmc$ symmetry. Also, the structure transition at high pressure is also predicted for MB_3 and MB_4 (M = Os and Ru). Moreover, among the borides, orthorhombic RuB_3 and OsB_4 phases are predicted to be potential hard materials with estimated Vickers hardness values of 26.3 and 31.3 GPa, respectively. The analysis on the electronic properties and crystal orbital Hamilton population shows that the directional boron–boron networks, together with the strong metal–boron bonds, are responsible for their excellent mechanical properties. Relative enthalpy calculations with respect to possible constituents are also investigated to assess the prospects for phase formation and an attempt at high-pressure synthesis is suggested to obtain osmium and ruthenium tri- and tetra-borides.

1. Introduction

Transition metal (TM) borides, as appealing candidates for hard or superhard materials,[1,2] have recently received noticeable attention. A variety of studies on Re–B,[3–5] W–B,[6] Mo–B[7] and Mn–B[8] systems revealed that the arrangement of the boron atoms (two-dimensional layers or three-dimensional networks) plays an important role in the mechanical properties of these borides. Among these systems, ReB_2, WB_2, MoB_3 and MnB_4 have been proposed as potentially hard or superhard materials due to their exceptionally high shear moduli. These systematical efforts help to understand the relationship between the structural features and electronic structures,

which can be used as a guide to optimize the mechanical properties through fine tuning the boron concentrations in these TM borides.

Recently, osmium di-boride (OsB_2) was synthesized at ambient conditions[9] and the incorporation of boron into the osmium lattice gives rise to a significant enhancement of the Vickers hardness (from 4 GPa for Os to 20 GPa for OsB_2). Furthermore, OsB and Os_2B_3 were prepared by arc melting and subsequent annealing at ambient pressure and the related mechanical properties were investigated.[10,11] In the Ru–B system, Ru_7B_3, RuB, Ru_2B_3 and RuB_2 were obtained experimentally.[10–12] The combination of noticeable mechanical properties and the low-cost synthesis condition suggests that Os and Ru borides may be good candidates for hard materials. Nevertheless, limited information on these borides with a high boron content is available both theoretically and experimentally. The OsB_3 phase with the space group $P\bar{6}m2$ was predicted using the USPEX code.[13] Additionally, Zhang et al.[14] predicted an orthorhombic $Pmmn$ OsB_4 phase with a theoretical Vickers hardness of 28 GPa using the CALYPSO code.[15] For Ru borides, RuB_4 with a $Pnnm$ structure was also theoretically investigated.[16] These results show that the introduction of more boron further strengthens the mechanical properties of Os borides. Although progress has been made to find the possible stable structures for Os and Ru borides,

[a]Key Laboratory of Metastable Materials Science and Technology, College of Material Science and Engineering, Yanshan University, Qinhuangdao 066004, China. E-mail: zjw@ysu.edu.cn, huiyang.gou@gmail.com, huiyang.gou@uni-bayreuth.de
[b]Research Center for Solid State Physics and Materials, School of Mathematics and Physics, Suzhou University of Science and Technology, Suzhou 215009, China
[c]Department of Chemistry and Chemical Biology, McMaster University, Hamilton, Ontario L8S 4M1, Canada
[d]Bayerisches Geoinstitut, Universität Bayreuth, D-95440 Bayreuth, Germany
[e]Material Physics and Technology at Extreme Conditions, Laboratory of Crystallography, University of Bayreuth, 95440 Bayreuth, Germany
†Electronic supplementary information (ESI) available. See DOI: 10.1039/c3dt32918f

systematical comparisons between different predictions are still sparse because their properties can completely alter with the presence of new structures. Moreover, in Os–B and Ru–B systems, for now we have a lack of knowledge of the reliable physical properties of all competing phases compared with previous borides and a clear picture of how to tune or control the mechanical properties to obtain compounds with higher boron concentrations. Therefore, a more detailed exploration of the structural features, relative stabilities and mechanical properties of borides, especially those with a high boron content, in Os–B and Ru–B systems is of great importance for potential technological applications. Furthermore, attempting to synthesize the predicted new compounds remains difficult and challenging in experiments and a possible synthesis route can help to further actual realization in the laboratory.

In this paper, we systematically explore the crystal structure, relatively stability and electronic structure of M_7B_3, MB, M_2B_3, MB_2, MB_3 and MB_4 (M = Os and Ru) to present a thorough understanding of Os–B and Ru–B systems. Additionally, possible synthesizing routes for MB_3 and MB_4 from their constituent elements and/or compounds are probed. Furthermore, the dynamic stability of the potential ground states found for MB_3 and MB_4 are studied by phonon dispersion. Also, their elastic moduli are calculated and their theoretical hardness is predicted. Finally, their structural features and bonding situations are analyzed from the electronic structure, distributions of electron density and crystal orbital Hamilton population (COHP). Therefore, the present results could provide a theoretical prerequisite for the experimental synthesis and technological applications of osmium and ruthenium borides.

2. Computational details

In the present work, the experimentally determined structures, Ru_7B_3 (No. 186, $P6_3mc$),[17] OsB (No. 187, $P\bar{6}m2$)[10] and hexagonal Ru_2B_3 (No. 194, $P6_3/mmc$)[18] structures were selected for M_7B_3, MB and M_2B_3, respectively. For MB_2, besides the experimentally examined orthorhombic OsB_2 (No. 59, $Pnma$),[10] the ReB_2 (No. 194, $P6_3/mmc$)[4] structure was also considered (denoted as 59- and 194-MB_2, respectively, hereafter). For MB_3 and MB_4, since no experimental structural results have been determined to date, we thus considered the predicted structures *via* the *ab initio* evolutionary algorithm in ref. 13 and 14 as well as some other possible structures. The orthorhombic TcP_3 (No. 62, $Pnma$),[19] FeB_3 (No. 11, $P2_1/m$)[20] and rhombohedral MoB_3 (No. 166, $R\bar{3}m$)[7] structures were considered for the MB_3 phases (designated as 62-, 11- and 166-MB_3, respectively, hereafter). For the MB_4 phases, five possible structures were adopted here, orthorhombic OsB_4 (No. 59, $Pmmn$),[14] hexagonal MoB_4 (No. 194, $P6_3/mmc$, Z = 2),[7] orthorhombic $oI10$-FeB_4 (No. 71, $Immm$),[19] and CrB_4 (No. 58, $Pnnm$)[15] (designated as 59-, 194-, 71- and 58-MB_4, respectively, hereafter), together with WB_4-type (No. 194, $P6_3/mmc$, Z = 4).[21]

Geometry optimization was performed using the CASTEP code[22] within the generalized gradient approximation of Perdew, Burke and Ernzerhof (GGA-PBE).[23] The optimization of the structural parameters and atomic positions were realized by minimizing the forces and stress tensors, and the interactions between the ions and the electrons of M and B were expressed by a Vanderbilt ultrasoft pseudopotential.[24] The cutoff energy of the atomic wave functions was set to be 400 eV and the k points, $8 \times 8 \times 6$, $10 \times 10 \times 10$, $10 \times 10 \times 4$, $10 \times 10 \times 6$ and $10 \times 10 \times 6$ were selected for M_7B_3, MB, M_2B_3, 59-MB_2 and 194-MB_2, respectively. A $10 \times 10 \times 10$ k point and cutoff energy of 450 eV were used for all the considered MB_3 and MB_4 phases to be precise enough for good energy convergence. Within each self-consistency cycle, the total energy was converged to be within 10^{-7} eV. The formation enthalpy of these borides was estimated by the following equation,[25] $\Delta H_f = [E_{total}(M_xB_y) - (xE_{total}(M) + yE_{total}(B))]/(x + y)$ (M = Os and Ru), where $E_{total}(M_xB_y)$ is the obtained total energies for the considered borides at equilibrium volume, $E_{total}(M)$ and $E_{total}(B)$ are the total energy of the pure hexagonal metal and the most stable allotrope of crystalline boron (α-B) at zero pressure, respectively. The polycrystal elastic moduli have been estimated *via* a Voight–Reuss–Hill (VRH) approximation.[26]

To gain further information on the chemical bonding of the present MB_3 and MB_4 phases, we performed tight-bonding linear muffin-tin orbital computations with the aid of an atomic sphere approximation (ASA) (TB-LMTO-ASA program).[27] Then, the calculated COHP and density of state (DOS), weighted by the corresponding Hamilton matrix elements from the self consistent LMTO wave function, were presented by plotting –COHP (E) curves, where positive and negative values stand for bonding and anti-bonding states, respectively. The Fermi levels have been set to zero energy.

3. Results and discussion

3.1 Structure features

The optimized equilibrium lattice parameters, relative total energy and the whole set of single crystal elastic constants (C_{ij}) for the considered Os and Ru borides are listed in Table 1. The obtained lattice parameters of Ru_7B_3, MB, M_2B_3 and 59-MB_2 (M = Os and Ru) are in good agreement with the available experimental results,[10,17,18] verifying the reliability of the calculation here. The obtained elastic constants of the studied structures are found to satisfy the Born–Huang mechanical stability criteria,[28–30] indicating their mechanical stabilities.

To gain systematical comprehension of the structural features, the optimized structures of M_7B_3, MB and M_2B_3 as well as 59- and 194-MB_2 (M = Os and Ru) are shown in Fig. 1 (for more the detailed bonding lengths in these compounds, please refer to the ESI†). The M_7B_3 structure (Fig. 1a) has a densely packed metal skeleton mainly composed of M tetrahedra and octahedra, while the B atoms occupy trigonal prism voids between the M tetrahedra and octahedra.[17] In this structure, the low B concentration fails to cut off the connection between the metal atoms (Fig. 1f). Therefore, there are still a large amount of M–M bonds whose distances are only slightly

Table 1 Calculated equilibrium lattice parameters, a_0 (Å), b_0 (Å), c_0 (Å), the difference in total energy, ΔE (eV) and elastic constants C_{ij} for the Os–B and Ru–B system

		a_0	b_0	c_0	ΔE	C_{11}	C_{22}	C_{33}	C_{44}	C_{55}	C_{66}	C_{12}	C_{13}
Os_7B_3	GGA	7.558		4.801		487		559	89			303	226
OsB	GGA	2.892		2.877		615		808	190			201	175
	Exp.[a]	2.876		2.871		618[b]		791	188			196	191
Os_2B_3	GGA	2.912		12.777		528		865	209			186	189
	Exp.[a]	2.909		12.945									
59-OsB_2	GGA	4.696		4.094	0	549	538	744	77	203	199	164	183
	Exp.[a]	4.686		4.082		546[b]	553	763	64	209	207	183	198
194-OsB_2	GGA	2.938		7.325	0.02	453		870	206			183	218
11-OsB_3	GGA	4.051	2.899	5.934	0	674	525	584	135	291	128	97	247
62-OsB_3	GGA	10.096	2.883	4.703	0.11	543	538	501	244	229	187	113	245
187-OsB_3	GGA	2.8952		4.609	0.17	519		733	189			126	219
	GGA[c]	2.903		4.616		525		751	186			125	221
166-OsB_3	GGA	5.287		9.072	0.35								
59-OsB_4	GGA	7.104	2.886	4.006	0	610	573	632	151	342	180	130	245
	GGA[d]	7.119	2.896	4.015		612	576	630	152	349	178	128	245
194-OsB_4	GGA	2.957		10.665	0.2	449		900	152			147	177
58-OsB_4	GGA	4.711	5.552	3.229	0.78								
71-OsB_4	GGA	4.698	3.289	5.547	0.81								
Ru_7B_3	GGA	7.497		4.731		401		374	94			178	164
	Exp.[e]	7.463		4.714									
RuB	GGA	2.866		2.855		505		704	160			189	160
	Exp.[a]	2.851		2.855									
Ru_2B_3	GGA	2.917		12.801		468		787	190			189	152
	Exp.[f]	2.905		12.812									
59-RuB_2	GGA	4.662		4.052	0	521	455	705	104	217	177	175	151
	Exp.[a]	4.645		4.045		518[g]		687	99			183	164
194-$RuB2$	GGA	2.918		7.272	0.02	453		822	203			188	156
62-RuB_3	GGA	4.033	2.894	5.857	0	497	462	471	224	219	187	111	229
11-RuB_3	GGA	9.996	2.866	4.696	0.07								
187-RuB_3	GGA	2.899		4.565	0.12	435		641	181			129	207
166-RuB_3	GGA	5.261		8.999	0.58								
194-RuB_4	GGA	2.943		10.59	0	442		830	162			150	152
59-RuB_4	GGA	7.059	2.872	3.988	0.17								
58-RuB_4	GGA	4.752	5.53	3.124	0.57	384	789	309	114	164	191	167	202
	GGA[h]					390	785	338	97	179	188	171	195
71-RuB_4	GGA	5.519	3.192	4.754	0.65								

[a] Ref. 10. [b] Ref. 35. [c] Ref. 13. [d] Ref. 14. [e] Ref. 17. [f] Ref. 18. [g] Ref. 36. [h] Ref. 16.
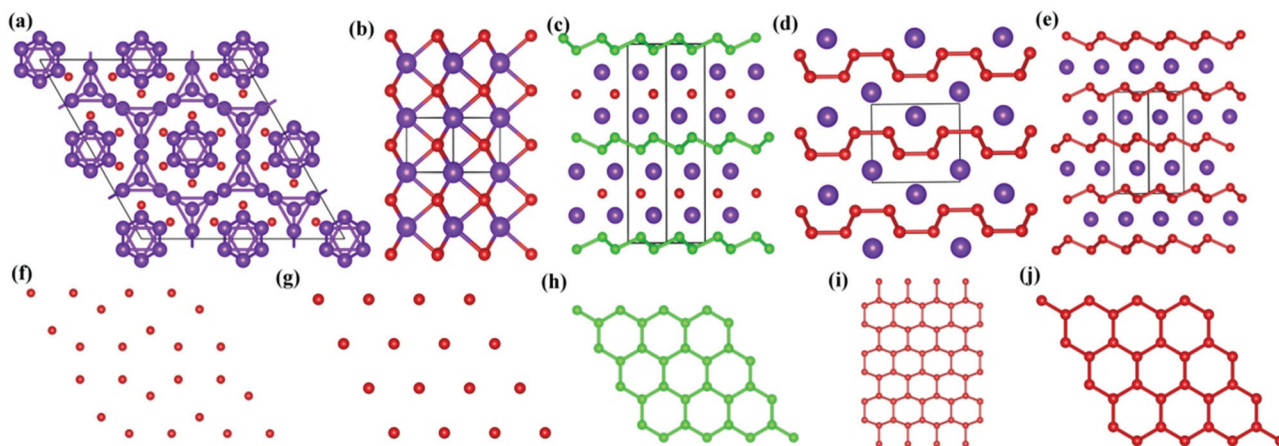

Fig. 1 Crystal structure for M_7B_3 (a), MB (b), M_2B_3 (c), 59-MB_2 (d), 194-MB_2 (e) and the corresponding configuration of the B layers appears (f–j) in these structures. The large purple spheres represent M atoms and the small green and red spheres represent B atoms.

greater than that of the pure metal, *e.g.* 2.731–2.901 Å (Os_7B_3) *vs.* 2.689 Å (Os), which may reserve its relatively high bulk modulus and low shear modulus, almost the same as metal Os. Furthermore, there are no directional B–B bonds in this structure. For MB, M_2B_3, 59-MB_2 and 194-MB_2, a common feature is the alternately stacking M and B layers along the

c-axis. In MB (Fig. 1b), the B atoms are situated at the center of trigonal M prisms and zig-zag tri-chains of M–B bonds form along the *c*-axis, giving rise to a particularly strong covalent M–B bond and thus corresponds to its high incompressibility along the *c*-axis.[10] Due to the long distances between the B atoms (exceeding 2.87 Å), no directional B–B bonds are formed either in or between the flat B layers of MB (Fig. 1g), in line with the COHP results reported in ref. 11. On adding more B to form M_2B_3 (Fig. 1c), the directional B–B bonds appear within puckered B layers (Fig. 1h). The B atoms (green) within the puckered layers are seven-coordinate with three B–B bonds (1.872 Å for Os_2B_3 and 1.857 Å for Ru_2B_3) and four M–B bonds. Nevertheless, the B atoms (red) in the flat layers remains the same as those in MB (Fig. 1g), coordinated by six M atoms at the corners of trigonal prisms. The M–B distances in M_2B_3 are slightly greater than those of MB (2.215 Å (Os_2B_3) *vs.* 2.204 Å (OsB) and 2.197 Å (Ru_2B_3) *vs.* 2.185 Å (RuB)). With this change in the trend of the B layers in hand, we then wondered whether all the B layers will evolve into a puckered configuration if the B content is further increases. This speculation indeed proves to be the case. Such a structure has been found to exist in 194-symmetry (Fig. 1e). All the B atoms have the same coordination as those of the green B atoms in M_2B_3 (Fig. 1j), with shorter B–B distance (1.861 Å for OsB_2 and 1.844 Å for RuB_2) but longer M–B bonding (2.230 Å for OsB_2 and 2.218 Å for RuB_2) than that of M_2B_3. However, as indicated by its positive energy with respect to 59-MB_2, 194-MB_2 is energetically unfavorable but turns out to be a high pressure phase of 59-MB_2, which will be discussed later. For 59-MB_2, B layers composed of hexagonal boat-like rings (Fig. 1d) are alternately stacking with folding M layers along the *c* direction. The B atoms also have sevenfold coordination (3B + 4M) with B–B distances of 1.817–1.908 Å for 59-OsB_2 and 1.816–1.887 Å for 59-RuB_2 (Fig. 1i). Differing from the MB structure, the covalent M–B bonds and directional B–B bonds both contribute to the zig-zag tri-chains along the *c*-axis in M_2B_3 and 194-MB_2. Nevertheless, there is still no directional B–B bond between the adjacent B layers in these phases.

Among all the considered structures for MB_3, the results of calculations for the total energy suggest that OsB_3 and RuB_3 have different potential ground state structures, possessing monoclinic $P2_1/m$ symmetry (11-OsB_3) and orthorhombic *Pnma* symmetry (62-RuB_3), respectively. Note that 11-OsB_3 is energetically more favorable than the previously proposed hexagonal $P\bar{6}m2$ structure. Similarly, the hexagonal $P6_3/mmc$ structure (194-RuB_4) is uncovered with the lowest total energy, favored over the previous prediction for orthorhombic RuB_4.[16] To further check the dynamic stability of the newly predicted low-energy structures, the phonon spectra are presented in Fig. 2. The absence of imaginary frequencies in the Brillouin Zone suggests that the predicted structures for MB_3 (M = Os and Ru) and 194-RuB_4 are dynamically stable.

To obtain further structure features of MB_3 and MB_4 (M = Os and Ru), the crystal structures of the potential ground state structures are illustrated in Fig. 3. Contrary to the puckered two-dimensional boron layers of the 59-OsB_2 phase, a three-dimensional (3D) B network forms in the 62-RuB_3, 11-OsB_3 and 59-OsB_4 structures and M atoms locate at the channels of the B network (Fig. 3a–c, respectively). In 62-RuB_3, the honeycomb ring in the B layer (*bc* plane) (Fig. 3e) resembles the counterpart B layer in 59-OsB_2 but with a much greater degree of undulation. These B layers were connected by zig-zag B–B (red) chains that lie parallel with the layers along the *b*-axis and the connecting sites in the B honeycomb locate at B–B bonds parallel with the *c*-axis. In 11-OsB_3, B honeycomb layers are also connected by zig-zag B–B (red) chains similar to 62-RuB_3, however, the connecting sites change to B–B bonds that are at an angle with the *c*-axis but half of these sites remain unconnected due to the limit of the B content, giving rise to a distortion of the B honeycomb. As the B content increases further to form 59-OsB_4, a similar scenario of connections between B layers happens but all of the connecting sites that are similar to 11-OsB_3 are connected, leading to a much more symmetrical B honeycomb. For the 62-RuB_3, 11-OsB_3 and 59-OsB_4 phases, the coordination of M atoms bears a close resemblance to the 59-MB_2 structure, in which M atoms nestle into boat-like B atomic six-rings. For the 194-RuB_4 structure (Fig. 3d), however, a 3D B network could not been found and the B (green and red B) layers that are comprised of two sub-layers of honeycomb B rings (Fig. 3h) are alternately stacking with M layers along the *c*-axis. A connection between the B layers is absent due to the large distance (2.771 Å) between them but the two B sub-layers are interconnected by short B–B bonds (1.685 Å and 1.895 Å).

3.2 Relative stability

To assess the thermodynamic stability of these Os and Ru phases, the formation enthalpy (ΔH_f) was calculated and diagrams of the convex hull are constructed. A negative ΔH_f for a structure provides inferences regarding the thermodynamic stability with respect to the elemental constituents.[24] As shown in Fig. 4a, the negative formation enthalpy of OsB, Os_2B_3, 59-OsB_2, 11-OsB_3 and 59-OsB_4 suggest that these phases could be synthesized at ambient conditions, which is confirmed by the experimental synthesis of OsB, Os_2B_3, 59-OsB_2.[10] However, the positive values for the formation enthalpy of Os_7B_3, 166-OsB_3, 71- and 58-OsB_4 imply that they are thermodynamically unstable with respect to the initial reactants. Furthermore, the theoretical WB_4-type OsB_4 proposed earlier[31] is also unstable as hinted by its large positive formation enthalpies (0.724 eV per atom). For Ru borides (Fig. 4b), the negative values of the formation energy of the Ru_7B_3, RuB, Ru_2B_3 and 59-RuB_2 phases validate the feasibility of solid state synthesis in experiments.[10,12] Moreover, 62-RuB_3 and 194-RuB_4 also show the negative values of the formation energy, opening the possibility of phase formation by the usually solid synthesis at ambient conditions.

Since extra pressure in the synthesis process of a compound could enhance its thermodynamic stability or the reaction kinetics and thus promote its formation in the predicted configurations[32] and promotes the understanding of the stability of higher boron Os– and Ru–B phases relative to lower boron
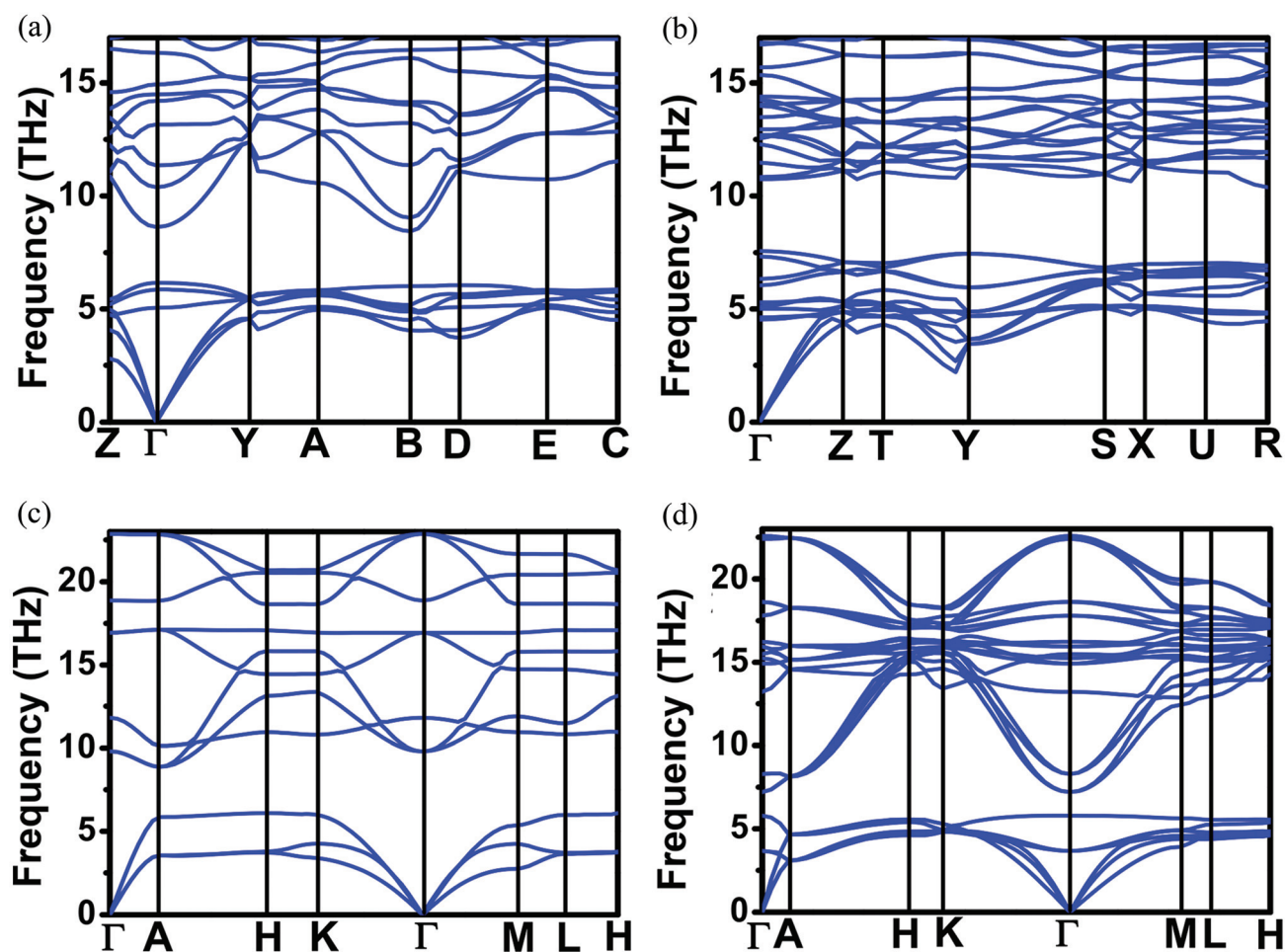
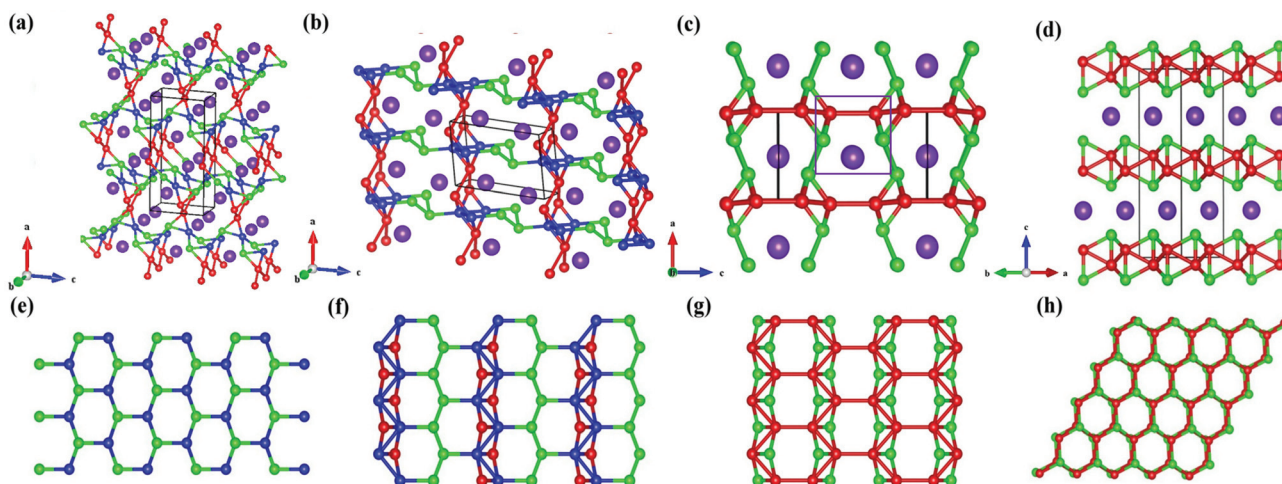**Fig. 2** Phonon dispersion for 62-RuB$_3$ (a), 11-OsB$_3$ (b), 187-OsB$_3$ (c) and 194-RuB$_4$ (d).

Fig. 3 Crystal structures for 62-RuB$_3$, where the Ru atoms occupy 4c (0.1055, 1/4, 0.1566) and the B atoms occupy the 4c (0.8199, 1/4, 0.1950), 4c (0.7861, 1/4, 0.5753) and 4c (0.4463, 1/4, 0.0222) positions (a), 11-OsB$_3$, where Os occupies 2e (0.9168, 1/4, 0.6967) and the B atoms occupy the 2e (0.2005, 1/4, 0.0566), 2e (0.3801, 1/4, 0.5478) and 2e (0.4873, 1/4, 0.8909) positions (b), 59-OsB$_4$, where the Os atoms occupy 2b (0, 0.5, 0.5409) and the B atoms occupy the 4f (0.2021, 0, 0.3076) and 4f (0.3461, 0, 0.9841) positions (c), 194-RuB$_4$, where the Ru atoms occupy 2d (2/3, 1/3, 1/4) and the B atoms occupy the 4f (1/3, 2/3, 0.1192) and 4f (2/3, 1/3, 0.0399) positions (d) and their B atomic configurations (e–h). The large purple spheres represent Os or Ru atoms and the small green, blue and red spheres represent B atoms.
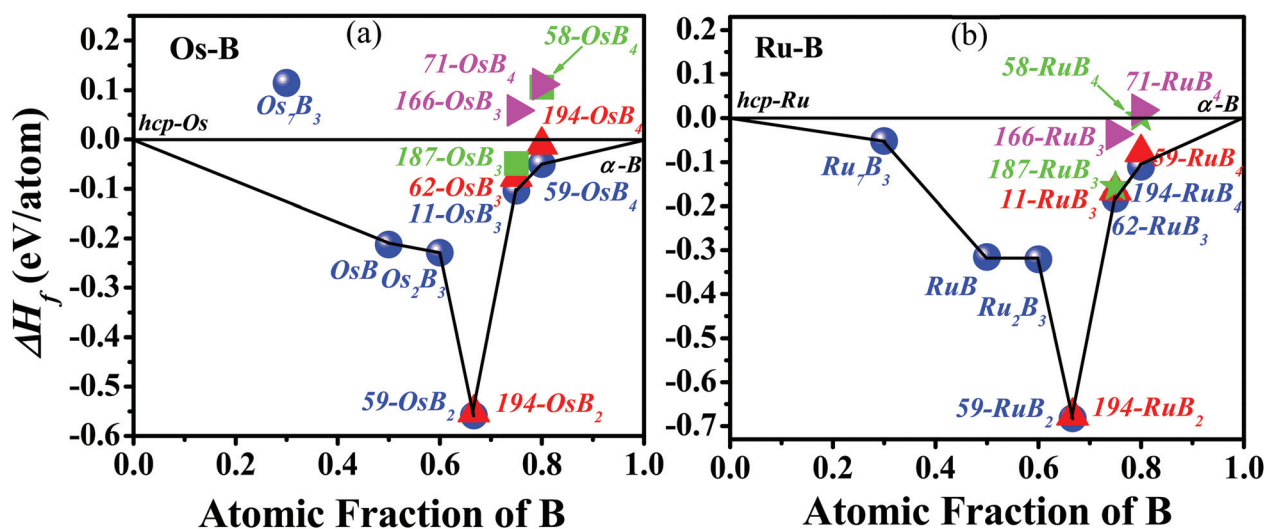
This journal is © The Royal Society of Chemistry 2013

Fig. 4 Convex hulls of the Os–B system (a) and Ru–B system (b) at zero pressure.

phases within a system, we further calculated the enthalpy difference between each boride and the possible reactant compositions under 0–50 GPa at zero temperature. For example, for 11-OsB$_3$, the possible reactants of Os + 3B, OsB + 2B, as well as 59- and 194-OsB$_2$ + B were considered. Here, two polymorphs of boron, α-B and γ-B were both considered at their pressure range, since γ-B is thermodynamically more favorable than any other known forms between 19 and 89 GPa.[33] This notion has been confirmed by the phase transition from α-B to γ-B at 19.3 GPa from Fig. 5, suggesting the credibility of our calculations.

All of the borides considered here are thermodynamically stable with respect to the pure metal and boron reactants under 0–50 GPa from Fig. 5. For MB$_2$, OsB$_2$ is more favorable than the mixtures of OsB and Os$_2$B$_3$ + α-B, consistent with the experimental result that OsB and Os$_2$B$_3$ can yield 59-OsB$_2$ with additional B atoms at ambient conditions.[9] Moreover, high pressure phase transition is identified for 59-OsB$_2$ (RuB$_2$) at 8.9 (8.3) GPa, above which 194-OsB$_2$ (RuB$_2$) is energetically more favorable. For MB$_3$ and MB$_4$ (M = Os and Ru), the MB$_2$ + B constituent in the entire range of the pressure is always favored energetically, indicating that the synthesis route of pure M + nB for MB$_3$ and MB$_4$ is inapplicable because the competitive phase of MB$_2$ will appear first. However, alternative synthesis routes from low boron content borides and metal is suggested to be feasible, as illustrated in Fig. 5. For Os borides, the 11-OsB$_3$ phase can be synthesized by OsB + α-B above 1.3 GPa or Os$_2$B$_3$ + α-B above 47 GPa and 59-OsB$_4$ may be obtained by OsB + α-B when exceeding 25 GPa. For Ru borides, 62-RuB$_3$ is found to be more energetically favorable than Ru$_2$B$_3$ + α-B above 16 GPa and 194-RuB$_4$ is more stable relative to RuB + α-B above 5.5 GPa and Ru$_2$B$_3$ + α-B exceeding 23 GPa. It is thus suggested that the combination of extra pressure and temperature could be more conductive to the phase formation of the MB$_3$ and MB$_4$ phases. Moreover, the

enthalpy calculations suggest that the phase transitions between 11- and 187-OsB$_3$, 59- and 194-OsB$_4$, as well as 62- and 187-RuB$_3$ happens at 43.3 GPa, 33.7 GPa and 39.5 GPa, respectively. 194-RuB$_4$ remains stable in the studied pressure range.

3.3 Mechanical properties

Besides mechanical stability, elastic constants (C_{ij}) (Table 1) can also be used to derive the elastic moduli and further predict theoretical hardness. The large value of C_{44} for 62-RuB$_3$ (224 GPa) and OsB$_3$ (244 GPa) indicates their stronger strength to resist shear deformation. Additionally, extremely large C_{33} values are found for the 194-OsB$_4$ (900 GPa) and 194-RuB$_4$ (830 GPa) phases, much greater than that of c-BN (773 GPa), suggesting their extremely high incompressibility along the c-axis.[34] Furthermore, the C_{11}, C_{22} and C_{33} values of 62-RuB$_3$, 62-OsB$_3$ and 59-OsB$_4$ are quite close to each other, thereby indicating their highly isotropic linear incompressibility.

The calculated bulk modulus, B, shear modulus, G, and Young's modulus, E, as listed in Table 2, as well as C_{ij} in Table 1 are all in reasonable agreement with the available results,[35,36] underlining the accuracy of our calculations. On moving from 59-OsB$_2$, 11-OsB$_3$ to 59-OsB$_4$, the B value decreases by 3.6% (11 GPa) and 3.3% (10 GPa), respectively. Also, for both Os–B and Ru–B systems, there is no monotone trend of the calculated B with VED (or boron content), *i.e.* B indirectly correlates to its VED (or boron content). Similar conclusions could be also reached from the Re–B[4] and Mo–B[7] systems. On the contrary, G shows a different changing trend from 59-OsB$_2$, 11-OsB$_3$ to 59-OsB$_4$, increasing by 26.2% (45 GPa) and 17% (31 GPa), respectively. This reveals that G is more sensitive to the boron content than B, similar to the Os–C compounds.[37] Moreover, 59-OsB$_4$ and 62-RuB$_3$ have maximum G values (217 GPa and 185 GPa, respectively) and minimum ν
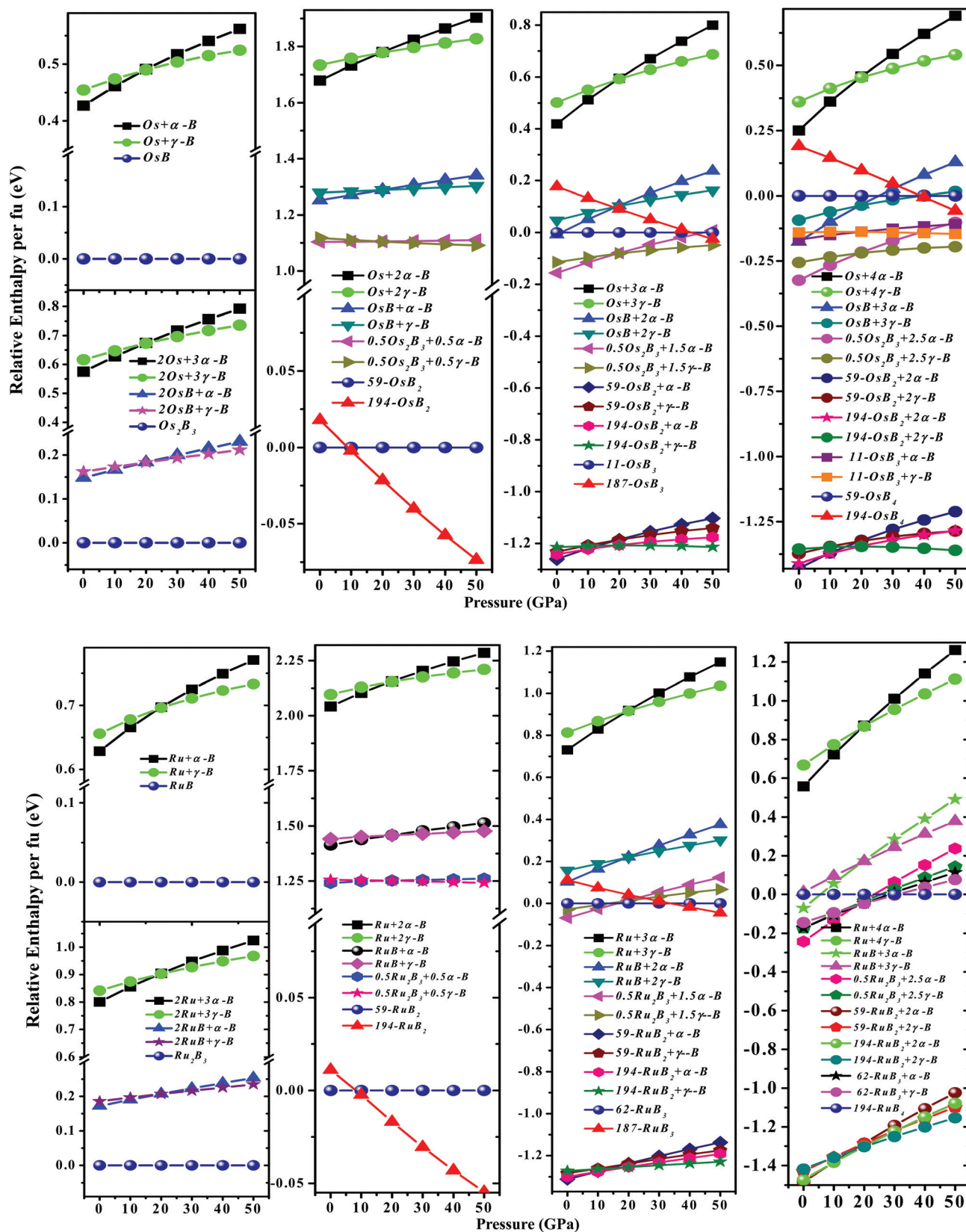
Fig. 5   Relative enthalpies between M–B (with stoichiometries of 1 : 1, 2 : 3, 1 : 2, 1 : 3, and 1 : 4) and the possible constituents under 0–50 GPa.

Table 2 Calculated valence electronic density (VED, e Å^{-3}), bulk modulus, B (GPa), shear modulus, G (GPa), Young's modulus, E (GPa), Poisson's ratio, v, Vickers hardness, H_v (GPa), and elastic isotropic index (A^U) for the Os–B and Ru–B compounds

		VED	B	G	G/B	E	v	H_v	A^U
59-OsB$_4$	GGA	0.4869	293	217	0.741	522	0.203	31.3	0.538
	GGA^a		294	218		524	0.204	28	
11-OsB$_3$	GGA	0.4972	303	186	0.614	463	0.245	25.1	0.653
59-OsB$_2$	GGA	0.5048	304	172	0.566	434	0.262	21.9	
	GGA^b		306	179	0.585			17.8–34.8^c	1.012
	GGA^d		307	168	0.547				
Os$_2$B$_3$	GGA	0.5329	331	201	0.607	501	0.247		0.25
OsB	GGA	0.5276	347	210	0.605	524	0.248		0.139
	GGA^d		350	212					
Os$_7$B$_3$	GGA	0.5467	338	103	0.305	281	0.362		
194-RuB$_4$	GGA	0.5037	281	175	0.623	435	0.242	23.5	0.408
62-RuB$_3$	GGA	0.5054	267	185	0.693	451	0.219	26.3	0.259
59-RuB$_2$	GGA	0.516	279	174	0.624	432	0.242	23.4	0.372
	GGA^b		280	175	0.625			14.4–24.2^e	
Ru$_2$B$_3$	GGA	0.518	296	178	0.601	445	0.25		0.373
RuB	GGA	0.5417	303	176	0.581	442	0.257		0.175
Ru$_7$B$_3$	GGA	0.5644	243	104	0.428	273	0.313		

^{a} Ref. 14. ^{b} Ref. 36. ^{c} Ref. 10 and 39. ^{d} Ref. 35. ^{e} Ref. 10 and 40.

(0.203 and 0.22, respectively), which suggests that strong directional bonding exists in these borides and thus could be potentially hard materials. Based on the empirical correlation ($H_v = 2 \ (k^2 G)^{0.583} - 3$),[38] we have estimated the Vickers hardness, H_v, of the MB$_3$ and MB$_4$ phases together with MB$_2$. The calculated H_v values of 59-OsB$_2$ and RuB$_2$ are in satisfactory agreement with previous experimental results.[10,39,40] Also, the estimated H_v for 59-OsB$_4$ of 31.3 GPa, is consistent with the available theoretical results (28 GPa) according to the Šimůnek model.[14] Besides 59-OsB$_4$, the boron-rich 11-OsB$_3$, 62-OsB$_3$ and 62-RuB$_3$ also show larger hardness values (25.1, 28.2 and 26.3 GPa, respectively) than that of 59-OsB$_2$ and RuB$_2$, implying that the higher boron-content compounds may be more likely to be potential hard materials or superhard films. On the other hand, the 62-OsB$_3$ and 59-OsB$_4$ (59-RuB$_4$) phases exhibit greater hardness compared with 11-OsB$_3$ and 194-OsB$_4$ (194-RuB$_4$), respectively. Thereby, it can be safely concluded that, besides the boron content, atomic configuration is another important factor to determine the mechanical property of a material.

The elastic anisotropy of materials has an important implication in engineering science since it is highly correlated with the possibility to induce microcracks in materials.[41] The elastic anisotropy of the borides considered here is estimated based on the universal elastic anisotropy index of $A^U = 5G^V/G^R + B^V/B^R - 6$,[42] where B and G denote the bulk and shear modulus and the superscripts V and R represent the Voigt and Reuss approximations. The calculated anisotropic indexes for the Os and Ru borides are listed in Table 2. It is noted that the anisotropy of the Os and Ru borides shows entirely different trends. In the Os–B system, the 59-OsB$_2$ phase is significantly anisotropic, which explains the big difference in the calculated ideal strength,[43] and 59-OsB$_4$ and 11-OsB$_3$ also exhibit some anisotropy to a certain degree. However, in the Ru–B system, 194-RuB$_4$ shows relatively strong

anisotropy, even greater than layered stacking 59-RuB$_2$, and 62-RuB$_3$ has a superior elastic isotropic character, as indicated by its smaller A^U value.[44]

3.4 Electronic structures

To address the general features of the stability and mechanical behavior of these borides, the DOSs and corresponding COHP are presented in Fig. 6. We can see that all the predicted MB$_3$ and MB$_4$ compounds show non-zero DOS values at the Fermi level ($N(E_F)$), exhibiting metallic behavior. Also, the M-d and B-2p states of all the considered borides overlap below the Fermi level, indicating the hybridization between the M-d and B-2p states and thus the presence of strong M–B bonding character. Compared to 59-OsB$_2$, a more extended overlap between the Os-d and B-2p orbital in the 11-OsB$_3$ phase indicates a relatively stronger covalent M–B bond. This can also be confirmed by the greater Mulliken overlap population (MOP) values of 11-OsB$_3$ (0.57 and 0.3) than 59-OsB$_2$ (0.51 and 0.15) because a greater MOP value corresponds to a higher degree of covalency in the bonding.[45] With the enhancement of the boron content, the Fermi level of 59-OsB$_4$ is found to locate in the pseudo-gap, suggesting high stability. Additionally, the calculated COHP shows that the Os–B interaction could be identified as the main functional bonding that stabilized $P\bar{6}m2$ OsB in view of its non-antibonding states found below the Fermi level.[10] However, with the increase of the boron content, the appearance of weak antibonding M–B interactions in MB$_2$, MB$_3$ and MB$_4$ may have a reverse influence on the stability. Fortunately, the relatively strong B–B bonding begins to form, as revealed by the positive –iCOHP values, and none of them show the antibonding interaction below the Fermi level, which, together with the reserved Os–B bonding, greatly compensates for the loss of stability from the Os–Os bonding. Furthermore, for 59-OsB$_4$, the weak antibonding (−0.135 eV per cell for the Os–Os interaction) restrains the rapid increase in the mechanical
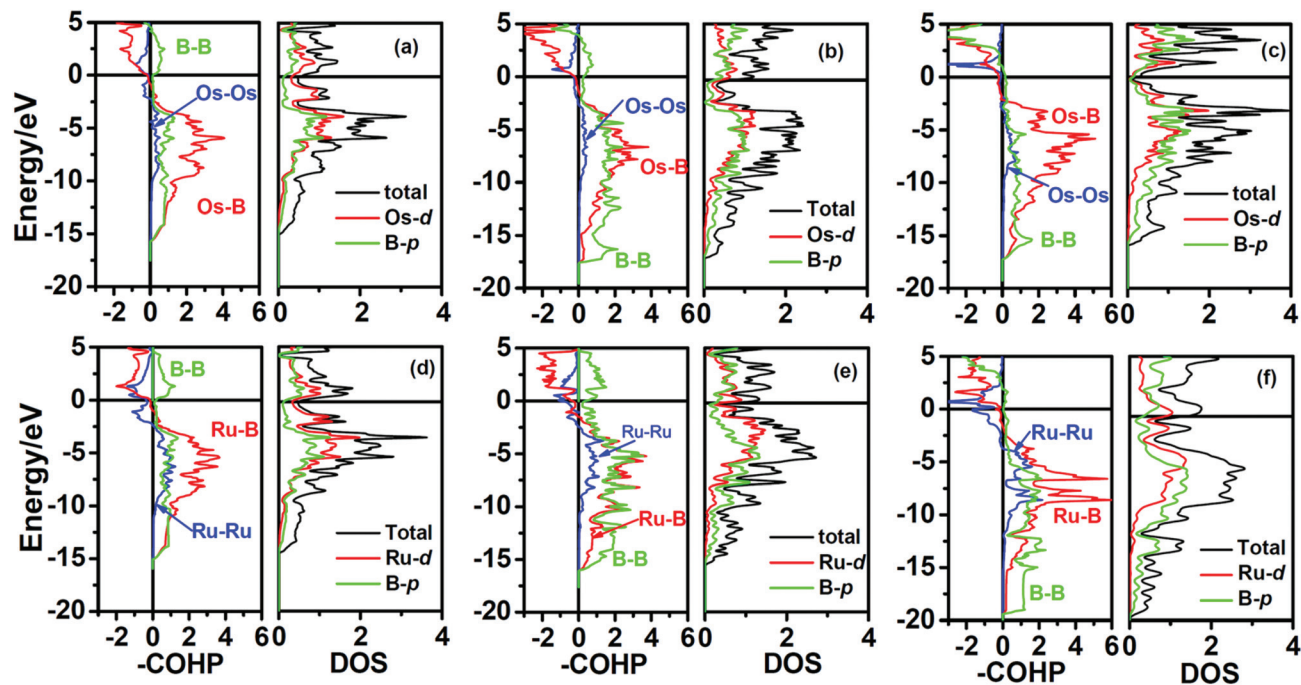
Fig. 6 DOS and –COHP curves for 59-OsB$_2$ (a), 11-OsB$_3$ (b), 59-OsB$_4$ (c), 59-RuB$_2$ (d), 62-RuB$_3$ (e) and 194-RuB$_4$ (f). In –COHP, a positive value is for a bonding interaction while a negative value is for an antibonding state.

properties, whereas for 194-RuB$_4$, the distinct anti-bonding (−0.95 eV per cell for Ru–Ru interaction) tends to weaken the mechanical properties compared with RuB$_3$.

4. Conclusion

The structural features, relative stability, possible synthesis routes, electronic structures and mechanical properties of Os–B and Ru–B systems were investigated *via* the first-principle techniques. The convex hull curves suggest that five Os–B phases (OsB, Os$_2$B$_3$, 59-OsB$_2$, 11-OsB$_3$ and 59-OsB$_4$) and six Ru–B phases (Ru$_7$B$_3$, RuB, Ru$_2$B$_3$, 59-RuB$_2$, 62-RuB$_3$ and 194-RuB$_4$) were thermodynamically stable at zero pressure. The total energy and phonon dispersion results indicate that the possible ground state structures at zero pressure are the $P2_1/m$, *Pnma* and $P6_3/mmc$ structures for OsB$_3$, RuB$_3$ and RuB$_4$, respectively. Furthermore, a phase transition was identified between 59- and 194-OsB$_2$(RuB$_2$), 11- and 187-OsB$_3$, 62- and 187-RuB$_3$, as well as 59- and 194-RuB$_4$. Among the Os–B and Ru–B compounds, 59-OsB$_4$ and 62-RuB$_3$ has the largest shear moduli, the lowest Poisson's ratio and an estimated Vickers hardness of 26.3 and 31.3 GPa, respectively. The origin of the excellent mechanical performance of 59-OsB$_4$ and 62-RuB$_3$, evidenced by the electronic properties and COHP, is the formation of directional boron–boron networks together with strong metal–boron bonds. Relative enthalpy calculations suggest that synthesis at high pressure is an applicable method to obtain osmium and ruthenium tri- and tetraborides.

References

1 A. L. Ivanovskii, *Prog. Mater. Sci.*, 2012, **57**, 184.

2 R. B. Kaner, J. J. Gilman and S. H. Tolbert, *Science*, 2005, **308**, 1268.

3 H. Y. Chung, M. B. Weinberger, J. B. Levine, A. Kavner, J. M. Yang, S. H. Tolbert and R. B. Kaner, *Science*, 2007, **316**, 436.

4 H. Y. Gou, Z. B. Wang, J. W. Zhang, S. T. Yan and F. M. Gao, *Inorg. Chem.*, 2009, **48**, 581.

5 E. J. Zhao, J. P. Wang, J. Meng and Z. J. Wu, *J. Comput. Chem.*, 2010, **31**, 1904.

6 E. J. Zhao, J. Meng, Y. M. Ma and Z. J. Wu, *Phys. Chem. Chem. Phys.*, 2010, **12**, 13158.

7 M. G. Zhang, H. Wang, H. B. Wang, T. Cui and Y. M. Ma, *J. Phys. Chem. C*, 2010, **114**, 6722.

8 B. Wang, X. Li, Y. X. Wang and Y. F. Tu, *J. Phys. Chem. C*, 2011, **115**, 21429.

9 R. W. Cumberland, M. B. Weinberger, J. J. Gilman, S. M. Clark, S. H. Tolbert and R. B. Kaner, *J. Am. Chem. Soc.*, 2005, **127**, 7264.

10 Q. F. Gu, G. Krauss and W. Steurer, *Adv. Mater.*, 2008, **20**, 3620.

11 B. P. T. Fokwa, P. R. N. Misse, M. Gilleβen and R. Dronskowski, *J. Alloys Compd.*, 2010, **489**, 339.

12 B. Aronsson, *Acta Chem. Scand.*, 1959, **13**, 109.

13 Z. W. Ji, C. C. Hu, D. H. Wang, Y. Zhong, J. Yang, W. Q. Zhang and H. Y. Zhou, *Acta Mater.*, 2012, **60**, 4208.

14 M. G. Zhang, H. Y. Yan, G. T. Zhang and H. Wang, *J. Phys. Chem. C*, 2012, **116**, 4293.

15 Y. C. Wang, J. Lv, L. Zhu and Y. M. Ma, *Phys. Rev. B: Condens. Matter Mater. Phys.*, 2010, **82**, 094116.

16 H. Y. Niu, J. Q. Wang, X. Q. Chen, D. Z. Li, Y. Y. Li, P. Lazar, R. Podloucky and A. N. Kolmogorov, *Phys. Rev. B: Condens. Matter Mater. Phys.*, 2012, **85**, 144116.

17 L. Fang, H. Yang, X. Y. Zhu, G. Wu, Z. S. Wang, L. Shan, C. Ren and H. H. Wen, *Phys. Rev. B: Condens. Matter Mater. Phys.*, 2009, **79**, 144509.

18 T. Lundstrom, *Ark. Kemi*, 1969, **30**, 115.

19 R. Rühl and W. Jeitschko, *Acta Crystallogr., Sect. B: Struct. Crystallogr. Cryst. Chem.*, 1982, **38**, 2784.

20 A. N. Kolmogorov, S. Shah, E. R. Margine, A. F. Bialon, T. Hammerschmidt and R. Drautz, *Phys. Rev. Lett.*, 2010, **105**, 217003.

21 P. A. Ramans and M. P. Krug, *Acta Crystallogr.*, 1966, **20**, 313.

22 M. Segall, P. Lindan, M. Probert, C. Pickard, P. Hasnip, S. Clark and M. Payne, *J. Phys.: Condens. Matter*, 2002, **14**, 2717.

23 J. P. Perdew and Y. Wang, *Phys. Rev. B: Condens. Matter*, 1992, **45**, 13244.

24 D. Vanderbilt, *Phys. Rev. B: Condens. Matter*, 1990, **41**, 7892.

25 G. L. Weerasinghe, R. J. Needs and C. J. Pickard, *Phys. Rev. B: Condens. Matter Mater. Phys.*, 2011, **84**, 174110.

26 R. Hill, *Proc. Phys. Soc., London, Sect. A*, 1952, **65**, 349.

27 R. Dronskowski and P. E. Blochl, *J. Phys. Chem.*, 1993, **97**, 8617.

28 M. Born, *Math. Proc. Cambridge Philos. Soc.*, 1940, **36**, 160.

29 M. Born and K. Huang, *Dynamical Theory of Crystal Lattices*, Clarendon, Oxford, 1956.

30 D. Wallace, *Thermodynamics of Crystals*, Wiley, New York, 1972.

31 M. Wang, Y. W. Li, T. Cui, Y. M. Ma and G. T. Zou, *Appl. Phys. Lett.*, 2008, **93**, 101905.

32 A. F. Bialon, T. Hammerschmidt, R. Drautz, S. Shah, E. R. Margine and A. N. Kolmogorov, *Appl. Phys. Lett.*, 2011, **98**, 081901.

33 A. R. Oganov, J. H. Chen, C. Gatti, Y. Z. Ma, Y. M. Ma, C. W. Glass, Z. X. Liu, T. Yu, O. O. Kurakevych and V. L. Solozhenko, *Nature*, 2009, **457**, 863.

34 X. F. Hao, Y. H. Xu, Z. J. Wu, D. F. Zhou, X. J. Liu, X. Q. Cao and J. Meng, *Phys. Rev. B: Condens. Matter Mater. Phys.*, 2006, **74**, 224112.

35 H. Y. Gou, L. Hou, J. W. Zhang, H. Li, G. F. Sun and F. M. Gao, *Appl. Phys. Lett.*, 2006, **88**, 221904.

36 J. Wang and Y. J. Wang, *J. Appl. Phys.*, 2009, **105**, 083539.

37 X. P. Du and Y. X. Wang, *J. Appl. Phys.*, 2010, **107**, 053506.

38 X. Q. Chen, H. Y. Niu, D. Z. Li and Y. Y. Li, *Intermetallics*, 2011, **19**, 1275.

39 H. Y. Chung, J. M. Yang, S. H. Tolbert and R. B. Kaner, *J. Mater. Res.*, 2008, **23**(6), 1797.

40 M. B. Weinberger, J. B. Levine, H. Y. Chung, R. W. Cumberland, H. I. Rasool, J. M. Yang, R. B. Kaner and S. H. Tolbert, *Chem. Mater.*, 2009, **21**, 1915.

41 P. Ravindran, L. Fast, P. A. Korzhavyi, B. Johnnsson, J. Wills and O. Eriksson, *J. Appl. Phys.*, 1998, **84**, 4891.

42 S. I. Ranganathan and M. Ostoja-Starzewski, *Phys. Rev. Lett.*, 2008, **101**, 055504.

43 J. Yang, H. Sun and C. F. Chen, *J. Am. Chem. Soc.*, 2008, **130**, 7200.

44 M. D. Segall, R. Shah, C. J. Pickard and M. C. Payne, *Phys. Rev. B: Condens. Matter*, 1996, **54**, 16317.

45 A. Knappschneider, C. Litterscheid, J. Kurzman, R. Seshadri and B. Albert, *Inorg. Chem.*, 2011, **50**, 10540.